Journal of Computational Physics **175,** 739–763 (2002)
doi:10.1006/jcph.2001.6965, available online at http://www.idealibrary.com on IDEAL®

An Explicit Fourth-Order Orthogonal Curvilinear Staggered-Grid FDTD Method for Maxwell's Equations

Zhongqiang Xie,* Chi-Hou Chan,† and Bo Zhang*,†

*School of Mathematical and Information Sciences, Coventry University, Coventry CV1 5FB, United Kingdom; and †Department of Electronic Engineering, City University of Hong Kong, Tat Chee Avenue, Kowloon, Hong Kong
E-mail: xie@coventry.ac.uk, eechic@cityu.edu.hk, and b.zhang@conventry.ac.uk

Received May 19, 2000; revised October 18, 2001

The explicit fourth-order staggered finite-difference time-domain scheme, previously proposed for a Cartesian grid, is extended to Maxwell's equations in an orthogonal curvilinear coordinate system and applied to electromagnetic wave problems. A simple technique is also presented for generating orthogonal curvilinear grids that conform to the material boundaries and interfaces of the problem. Numerical experiments are presented to illustrate the efficiency and accuracy of the method. © 2002 Elsevier Science (USA)

Key Words: Maxwell's equations; FDTD method; Yee's scheme; staggered scheme; explicit fourth-order scheme; orthogonal curvilinear grid.

1. INTRODUCTION

The finite-difference time-domain (FDTD) method, which was first introduced by Yee [55] in 1966 and later developed by Taflove and others [43–46] and which employs a fully staggered space–time grid, is a very efficient numerical algorithm in computational electromagnetics and is applicable to a broad range of problems. However, the traditional FDTD scheme is based on a Cartesian coordinate system, and it is difficult to exactly generate grids for electromagnetic structures with curved boundaries and interfaces. The usual and straightforward approach is to simply approximate the boundaries and interfaces using a staircased curve, and an accurate solution can only be obtained using very fine grids and, consequently, a very small time step. While this may seem adequate for many problems it nevertheless affects the overall accuracy and essentially reduces the (second-order) Yee scheme to first order (see, e.g., [10, 29, 43, 44]). In the case of perfectly conducting boundaries this problem has been considered by many authors (see, e.g., [10, 29]), and a

0021-9991/02 $35.00

number of approaches have also been put forward to tackle the problem: nonorthogonal curvilinear FDTD methods [22, 28, 35], contour path methods [27, 31], locally conformal FDTD methods [21, 26, 56], and finite-element or finite-volume methods on unstructured grids [6, 37, 38, 57]. A variety of other techniques can be found in [43, 44]. Most, if not all, of these methods, however, sacrifice the simplicity of the original Yee scheme to achieve the improved accuracy, and moreover they are difficult to extend to high-order schemes.

In the case of dielectric interfaces where the tangential components of the electric field is nonzero, additional difficulties arise when imposing the interface conditions on curved interfaces with nonorthogonal curvilinear or unstructured grids, and few results are available. For the scalar wave equation with a general curvilinear interface a second-order immersed interface method was proposed in [36], in which a simple Cartesian grid is maintained and the finite-difference stencils around the immersed interfaces are modified to account for the correct position of the interface and the proper physical jump-conditions. The contour path method was extended in [27] to deal with electromagnetic scattering by random rough interfaces. In [18], a block pseudospectral method was proposed for Maxwell's equations with discontinuous coefficients, and proper physical jump-conditions at interfaces were also used to couple blocks via fictitious points or a generalization of characteristic outflow conditions in the case of a straight-line interface. Extension by a change of variable was also mentioned in [18] in the case of curvilinear interfaces.

On the other hand, the (second-order) Yee scheme has been widely used with a great deal of success. It is, however, efficient only for geometries of moderate electrical size. For wave propagation over longer distances, the grid resolution requirements of the Yee scheme can become excessive, leading to impractical CPU and memory requirements. One is thus naturally led to the development of higher-order schemes which produce smaller dispersion or phase errors for a given grid resolution [20, 41, 43, 44, 50, 53, 58–60]. Note that higher-order finite-difference schemes have also been developed for the elastic wave equation [8] as well as for acoustic applications (see, e.g., [16, 23] and the reference quoted there).

An important issue associated with high-order interior differencing schemes is the use of numerical boundary schemes which must be suitably accurate relative to the interior scheme [24, 25] and must be stable. This is because high-order difference schemes often have a large spatial stencil which cannot be used near boundaries and material discontinuities. Appropriate numerical boundary schemes can be difficult to obtain, and this represents a significant obstacle to the use of higher-order methods. Recent progress is reported by Carpenter *et al.* [12, 13], Turkel and Yefet [50], and Abarbanel *et al.* [1] in the case of perfectly conducting boundaries. However, in the case of dielectric interfaces only a few results are available. For a plane interface which coincides with the electric grid points, appropriate fourth-order accurate boundary schemes were derived near dielectric interfaces in [58] for an explicit fourth-order in space and second-order in time, staggered, FDTD scheme by using fourth-order accurate one-sided extrapolation and one-sided difference approximations. Similar treatment can be found in [59] for compact implicit fourth-order in both space and time schemes. In [53], in the case when the electric grid points coincide with the interface, third-order boundary schemes were given near flat dielectric interfaces for an explicit fourth-order in both space and time, staggered, FDTD scheme by making use of third-order one-sided difference approximations combined with the immersed interface technique. The third-order boundary treatment in [53] is numerically stable and does not affect the overall fourth-order accuracy of the scheme, as confirmed by numerical experiments.

Compared with previously developed fourth-order schemes, the FDTD scheme proposed in [53] is explicit, fourth-order accurate in both space and time, and employs the fully staggered, space and time grid, which is more efficient than nonstaggered grids [54]. Numerical experiments indicate that the scheme as well as its associated third-order boundary treatments is numerically stable and highly efficient (with respect to Yee's scheme). Another advantage is that the scheme retains much of the original simplicity of Yee's scheme and is easy to implement in conjunction with the reflectionless absorbing layers developed in, for example, [2, 9, 41] in simulating scattering of waves from computational domains. The disadvantage is that the scheme is based on a rectangular grid similar to the Yee scheme and hence is ineffeicient for complex structures.

In this paper we extend the fourth-order scheme in [53] to an orthogonal curvilinear grid which conforms to metallic boundaries and dielectric interfaces so it can be applied to complex electromagnetic structures. This is done in Section 2, where the associated third-order boundary schemes have also been described for two classes of boundary conditions: the dielectric interface and the perfect conductor. The third-order boundary schemes are derived using one-sided difference approximations combined with the immersed interface technique [36] and do not affect the overall fourth-order convergence rate of the fourth-order scheme, as confirmed by the numerical experiments in Section 3, which is consistent with the theorectical results of Gustafsson [24, 25]. The fourth-order scheme has also been extended to the reflectionless absorbing layer simulating radiation out of a computational domain. The advantage of using orthogonal curvilinear grids is that the simple structure of Maxwell's equations is remained in the transformed equations and the boundary and interface conditions are greatly simplified under orthogonal curvilinear grids (see Section 2) so that they are much easier to deal with numerically. Moreover, nonorthogonal grids may lead to numerical difficulties when cells are badly deformed [32]. Our orthogonal grid method can be applied to problems involving smooth duct-shaped domains, such as scattering by rough surfaces, including periodic surfaces (diffraction gratings), and wave propagation and scattering in multilayered media with smooth curved boundaries and interfaces.

On the other hand, orthogonal grids have limitations in applications due to the difficulty of generating orthogonal grids for problems involving sharp/nonsmooth features and/or boundaries and interfaces with significant variations. So orthogonal grid methods are not directly applicable in these cases but can be useful in combination with multidomain techniques, which will be investigated in the future.

It should be remarked that orthogonal grid generation has been studied by many authors in the two-dimensional case (see, e.g., [3, 5, 19, 32, 47, 49] and the references quoted there), including the case of doubly connected regions [52], and in the three-dimensional case [32, 48, 49]. Recently, orthogonal grids have also been used for numerically solving problems in duct acoustics in [4] and for electromagnetic wave propagation problems in multilayered regions with curved boundaries and interfaces in [34, 39].

A numerical example, which models a cylindrical PEC resonator consisting of two concentric PEC cylinders with an electromagnetic wave bouncing back and forth between the walls, is presented in Section 3.1 to illustrate the efficiency of the new scheme. The results indicate that the staircase approximation may not be appropriate in the computation of microwave resonators due to the fact that in this case an electromagnetic wave is bouncing back and forth between the walls, so numerical errors are building up very quickly in the solution. Instead, conformal orthogonal curvilinear grid schemes are appropriate alternatives. In Section 3.2 the new scheme is applied to scattering from periodic surfaces, and

numerical results indicate that the fourth-order scheme is numerically stable as well as accurate and efficient in modeling electromagnetic scattering from periodic surfaces. The orthogonal curvilinear grid that conforms to the material boundaries and interfaces in the scattering problem and is used in Section 3.2 was generated by a simple technique proposed in Appendix B.

2. MAXWELL'S EQUATIONS AND THE DISCRETIZATION

We restrict our descriptions to two-dimensional cases although extension to 3D is straightforward. Considering in this paper the transverse electric (TE) polarization case in an inhomogeneous, isotropic medium, the model equations in a Cartesian coordinate system are

$$\frac{\partial H^x}{\partial t} = -\frac{1}{\mu}\left(\frac{\partial E^z}{\partial y} + \sigma^M H^x\right), \tag{2.1}$$

$$\frac{\partial H^y}{\partial t} = \frac{1}{\mu}\left(\frac{\partial E^z}{\partial x} - \sigma^M H^y\right), \tag{2.2}$$

$$\frac{\partial E^z}{\partial t} = \frac{1}{\epsilon}\left(\frac{\partial H^y}{\partial x} - \frac{\partial H^x}{\partial y} - \sigma^E E^z\right), \tag{2.3}$$

where ϵ and μ are the permittivity and permeability, and σ^M and σ^E denote, respectively, the magnetic and electric losses of the medium.

We introduce the following coordinate transformation which transforms the computational domain in the physical space (i.e., (x, y)-plan) into a rectangular region in the transformed space (i.e., (ξ, η)-plan):

$$x = x(\xi, \eta), \quad y = y(\xi, \eta). \tag{2.4}$$

Then Maxwell's equations (2.1)–(2.3) are transformed into

$$\frac{\partial H^\xi}{\partial t} = -\frac{1}{J\mu}\frac{\partial E^z}{\partial \eta} - \frac{\sigma^M}{\mu}H^\xi, \tag{2.5}$$

$$\frac{\partial H^\eta}{\partial t} = \frac{1}{J\mu}\frac{\partial E^z}{\partial \xi} - \frac{\sigma^M}{\mu}H^\eta, \tag{2.6}$$

$$\frac{\partial E^z}{\partial t} = \frac{1}{J\epsilon}\left[\alpha\frac{\partial H^\eta}{\partial \xi} - \beta\frac{\partial H^\xi}{\partial \eta} - \gamma\left(\frac{\partial H^\eta}{\partial \eta} - \frac{\partial H^\xi}{\partial \xi}\right)\right] + \frac{1}{J\epsilon}\left(PH^\xi + QH^\eta\right) - \frac{\sigma^E}{\epsilon}E^z, \tag{2.7}$$

where $J = x_\xi y_\eta - x_\eta y_\xi$ is the Jacobian, $H^\xi = H^x\xi_x + H^y\xi_y$ and $H^\eta = H^x\eta_x + H^y\eta_y$ are the contravariant magnetic components, $\alpha = x_\eta^2 + y_\eta^2$ and $\beta = x_\xi^2 + y_\xi^2$ are the metrics, $\gamma = x_\xi x_\eta + y_\xi y_\eta$, and

$$P = y_{\xi\xi}y_\eta - y_{\xi\eta}y_\xi + x_{\xi\xi}x_\eta - x_{\xi\eta}x_\xi, \tag{2.8}$$

$$Q = y_{\eta\xi}y_\eta - y_{\eta\eta}y_\xi + x_{\eta\xi}x_\eta - x_{\eta\eta}x_\xi. \tag{2.9}$$

Here the subscripts ξ and η refer to the derivatives with respect to ξ and η, and by using the relationship

$$x_\xi = J\eta_y, \quad x_\eta = -J\xi_y, \quad y_\xi = -J\eta_x, \quad y_\eta = J\xi_x,$$

it follows that $H^x = H^\xi x_\xi + H^\eta x_\eta$ and $H^y = H^\xi y_\xi + H^\eta y_\eta$.

We assume that the above coordinate transformation is orthogonal (i.e., $\gamma = 0$ and $J \neq 0$), so that $\alpha > 0,\ \beta > 0$, and J does not change sign. Then (2.7) becomes

$$\frac{\partial E^z}{\partial t} = \frac{1}{J\epsilon}\left[\alpha\frac{\partial H^\eta}{\partial \xi} - \beta\frac{\partial H^\xi}{\partial \eta}\right] + \frac{1}{J\epsilon}(PH^\xi + QH^\eta) - \frac{\sigma^E}{\epsilon}E^z. \tag{2.10}$$

Thus, in the orthogonal curvilinear coordinate system (ξ, η) the transformed equations (2.5), (2.6), and (2.10) are of a structure similar to the original Maxwell's equations so that the fully staggered space-time grid, which is more efficient than the nonstaggered one [54], is applicable.

Orthogonality is a desirable property, since the metric tensor [32] of the transformation then has zero off-diagonal elements, which simplifies both the transformed equations and the application of boundary conditions, as seen above and below. A nonorthogonal transformation could be used, but finding a suitable discretization would be more complicated. Moreover, nonorthogonal grids may lead to numerical difficulties when cells are badly deformed [32]. Note that orthogonal curvilinear grids have been studied by many authors (see, e.g., [3, 5, 19, 32, 47–48, 49, 52] and the references quoted there) and employed to solve duct acoustic problems in [4] as well as problems of electromagnetic wave propagation in multilayed media with curved boundaries and interfaces in [34, 39].

2.1. Discretization

In [53], an explicit fourth-order accurate staggered FDTD scheme was proposed for Maxwell's equations in a Cartesian coordinate system, which is fourth-order accurate in both space and time, conditionally stable, and highly efficient (with respect to Yee's second-order accurate scheme) and still retains much of the original simplicity of Yee's scheme. The idea of deriving the fourth-order scheme in [53] was first to apply the Taylor expansion method to the temporal derivative so that a third-order correctional temporal derivative could be introduced in the discretization and then to reduce the third-order temporal derivative to the second-order by employing the Maxwell equations. The idea can be extended to the Maxwell equations (2.5), (2.6), and (2.10) in the orthogonal system (ξ, η). For example, consider the equation (2.5). From the Taylor expansion it follows that

$$\left.\frac{\partial H^\xi}{\partial t}\right|^n = \frac{H^\xi|^{n+1/2} - H^\xi|^{n-1/2}}{\delta t} - \frac{(\delta t)^2}{24}\left.\frac{\partial^3 H^\xi}{\partial t^3}\right|^n + O((\delta t)^4), \tag{2.11}$$

where δt is the time-step size and u^n denotes the value of u at $t = n\delta t$. Using Eq. (2.5) gives

$$\left.\frac{\partial^3 H^\xi}{\partial t^3}\right|^n = -\left.\frac{\partial^2}{\partial t^2}\left(\frac{1}{J\mu}\frac{\partial E^z}{\partial \eta} - \frac{\sigma^M}{\mu}H^\xi\right)\right|^n, \tag{2.12}$$

$$\left.\frac{\partial^2 H^\xi}{\partial t^2}\right|^n = -\frac{1}{J\mu}\left(\frac{\partial}{\partial t} - \frac{\sigma^M}{\mu}\right)\left.\left(\frac{\partial E^z}{\partial \eta}\right)\right|^n + \left(\frac{\sigma^M}{\mu}\right)^2 H^\xi|^n. \tag{2.13}$$

To make use of Yee's fully staggered space–time grid in the fourth-order scheme we can apply the fourth-order approximation to $H^{\xi}|^n$:

$$H^{\xi}|^n = \frac{H^{\xi}|^{n+1/2} + H^{\xi}|^{n-1/2}}{2} - \frac{(\delta t)^2}{8}\frac{\partial^2 H^{\xi}}{\partial t^2}\bigg|^n + O((\delta t)^4). \tag{2.14}$$

From (2.13) and (2.14) $H^{\xi}|^n$ and $(\partial^2 H^{\xi}/\partial t^2)|^n$ can be obtained, which together with (2.12), (2.11), and (2.5) implies that

$$\begin{aligned}(1+\tilde{\sigma}_M)\, H^{\xi}|^{n+1/2} = (1-\tilde{\sigma}_M)\, H^{\xi}|^{n-1/2} - \frac{\delta t}{J\mu}\Bigg[1 + \frac{(\delta t)^2}{24}\frac{\partial^2}{\partial t^2} + \frac{\bar{\sigma}_M}{12}\left(1+\frac{\bar{\sigma}_M^2}{8}\right)^{-1} \\ \times \left(\delta t\frac{\partial}{\partial t} - \bar{\sigma}_M\right)\Bigg]\left(\frac{\partial E^z}{\partial \eta}\right)\Bigg|^n,\end{aligned} \tag{2.15}$$

where $\bar{\sigma}_M = \sigma^M \delta t/\mu$ and $\tilde{\sigma}_M = \bar{\sigma}_M(1+\bar{\sigma}_M^2/8)^{-1}(1+\bar{\sigma}_M^2/24)/2$. Let us consider a uniform grid with grid sizes $\Delta\xi$ and $\Delta\eta$ on a rectangular region in the transformed space and assume that the grid is indexed by (i, j). To derive a fourth-order scheme we can apply the fourth-order centered difference approximation to the first-order spatial derivative $(\partial E^z/\partial\eta)$ and obtain that

$$\begin{aligned}\left(1+\tilde{\sigma}_M|_{i,j+1/2}\right) H^{\xi}\big|_{i,j+1/2}^{n+1/2} = \left(1-\tilde{\sigma}_M|_{i,j+1/2}\right) H^{\xi}\big|_{i,j+1/2}^{n-1/2} - \frac{\delta t}{(J\mu)|_{i,j+1/2}} \\ \times \Bigg[1 + \frac{(\delta t)^2}{24}\frac{\partial^2}{\partial t^2} + \frac{\bar{\sigma}_M|_{i,j+1/2}}{12}\left(1+\frac{1}{8}\bar{\sigma}_M^2\big|_{i,j+1/2}\right)^{-1} \\ \times \left(\delta t\frac{\partial}{\partial t} - \bar{\sigma}_M|_{i,j+1/2}\right)\Bigg]\left[\Lambda_\eta\left(E^z\big|_{i,j+1/2}^n\right)\right],\end{aligned} \tag{2.16}$$

where Λ_η denotes the fourth-order centered difference operator of the first-order spatial derivative along η, defined by

$$\Lambda_\eta(u_{i,j}) = \frac{1}{\Delta\eta}\left(\frac{1}{24}u_{i,j-3/2} - \frac{9}{8}u_{i,j-1/2} + \frac{9}{8}u_{i,j+1/2} - \frac{1}{24}u_{i,j+3/2}\right).$$

The discretization induces discrete values for all of the transformed variables in the Maxwell equations. For example,

$$u_{i,j}^n = u(t_n, \xi_i, \eta_j),$$

with $(\xi_i, \eta_j) = (i\Delta\xi, j\Delta\eta)$ being the grid points in the transformed domain and $t_n = n\delta t$ the time. The transformation (2.4) also carries the transformed-space grid to a physical-space grid $(x_{i,j}, y_{i,j})$, where $x_{i,j} = x(\xi_i, \eta_j)$ and $y_{i,j} = y(\xi_i, \eta_j)$.

For (2.6) and (2.10) a similar argument as above can be used to obtain that

$$\begin{aligned}
&\left(1+\tilde{\sigma}_M|_{i+1/2,j}\right) H^{\eta}\Big|_{i+1/2,j}^{n+1/2} \\
&\quad = \left(1-\tilde{\sigma}_M|_{i+1/2,j}\right) H^{\eta}\Big|_{i+1/2,j}^{n-1/2} + \frac{\delta t}{(J\mu)|_{i+1/2,j}} \left[1+\frac{(\delta t)^2}{24}\frac{\partial^2}{\partial t^2}+\frac{\bar{\sigma}_M|_{i+1/2,j}}{12}\right. \\
&\quad \left.\times\left(1+\frac{1}{8}\bar{\sigma}_M^2\Big|_{i+1/2,j}\right)^{-1}\left(\delta t\frac{\partial}{\partial t}-\bar{\sigma}_M|_{i+1/2,j}\right)\right]\left[\Lambda_{\xi}\left(E^z\big|_{i+1/2,j}^{n}\right)\right], \qquad (2.17)
\end{aligned}$$

$$\begin{aligned}
\left(1+\tilde{\sigma}_E|_{i,j}\right) E^z\Big|_{i,j}^{n+1} &= \left(1-\tilde{\sigma}_E|_{i,j}\right) E^z\Big|_{i,j}^{n} + \frac{\delta t}{(J\epsilon)|_{i,j}}\left[1+\frac{(\delta t)^2}{24}\frac{\partial^2}{\partial t^2}+\frac{\bar{\sigma}_E|_{i,j}}{12}\right. \\
&\quad \left.\times\left(1+\frac{1}{8}\bar{\sigma}_E^2\big|_{i,j}\right)^{-1}\left(\delta t\frac{\partial}{\partial t}-\bar{\sigma}_E|_{i,j}\right)\right] \\
&\quad \times\left[\alpha_{i,j}\Lambda_{\xi}\left(H^{\eta}\big|_{i,j}^{n+1/2}\right)-\beta_{i,j}\Lambda_{\eta}\left(H^{\xi}\big|_{i,j}^{n+1/2}\right)\right. \\
&\quad \left.+\left(P_{i,j}\,H^{\xi}\big|_{i,j}^{n+1/2}+Q_{i,j}\,H^{\eta}\big|_{i,j}^{n+1/2}\right)\right], \qquad (2.18)
\end{aligned}$$

where $\bar{\sigma}_E$ and $\tilde{\sigma}_E$ have expressions similar to $\bar{\sigma}_M$ and $\tilde{\sigma}_M$, with μ and the supscript M being replaced with ϵ and E, respectively, and where Λ_{ξ} denotes the fourth-order centered difference operator of the first-order spatial derivative along ξ, defined by

$$\Lambda_{\xi}(u_{i,j}) = \frac{1}{\Delta\xi}\left(\frac{1}{24}u_{i-3/2,j}-\frac{9}{8}u_{i-1/2,j}+\frac{9}{8}u_{i+1/2,j}-\frac{1}{24}u_{i+3/2,j}\right).$$

To obtain a fourth-order in both space and time scheme we employ the four-point second-order backward difference approximation

$$\frac{\partial^2 u^n}{\partial t^2} \approx \frac{1}{(\delta t)^2}(2u^n-5u^{n-1}+4u^{n-2}-u^{n-3})$$

and the four-point third-order backward difference approximation

$$\frac{\partial u^n}{\partial t} \approx \frac{1}{3\delta t}(10u^n-18u^{n-1}+9u^{n-2}-u^{n-3})$$

for the second- and first-order temporal derivatives, respectively, which appear in (2.18), (2.16), and (2.17). On the other hand, on a spatially staggered grid the values of H_{ξ} and H_{η} at integer grid points (i, j) are not defined directly, and the following fourth-order interpolations may be used:

$$\begin{aligned}
H_{i,j}^{\xi} &= \frac{1}{16}\left(-H_{i,j-3/2}^{\xi}+9H_{i,j-1/2}^{\xi}+9H_{i,j+1/2}^{\xi}-H_{i,j+3/2}^{\xi}\right), \\
H_{i,j}^{\eta} &= \frac{1}{16}\left(-H_{i-3/2,j}^{\xi}+9H_{i-1/2,j}^{\xi}+9H_{i+1/2,j}^{\xi}-H_{i+3/2,j}^{\xi}\right).
\end{aligned}$$

Finally, the discrete values at the grid points (i, j) of the coefficients in (2.18) (i.e., $\alpha_{i,j}$, $\beta_{i,j}$, $P_{i,j}$, and $Q_{i,j}$) involve those of the derivatives of x and y with respect to ξ and η. As is seen in Appendix B, the calculation of the second-order derivatives is reduced to that of

the two simplest first-order grid derivatives x_ξ and y_η, which may be approximated by the five-point fourth-order centered difference schemes

$$x_\xi|_{i,j} = \frac{1}{12\Delta\xi}(x_{i-2,j} - 8x_{i-1,j} + 8x_{i+1,j} - x_{i+2,j}), \tag{2.19}$$

$$y_\eta|_{i,j} = \frac{1}{12\Delta\eta}(y_{i,j-2} - 8y_{i,j-1} + 8y_{i,j+1} - y_{i,j+2}). \tag{2.20}$$

The above explicit fourth-order in both space and time leapfrog FDTD scheme needs the history values of the field unknowns at four time levels. Compared with the Yee scheme the fourth-order scheme requires additional computational memory but does not increase the workload sharply. In fact, as illustrated in Appendix A and the numerical experiments in Section 3.2 (see Table II below), to achieve the same level of numerical error the CPU time and memory requirements of the Yee scheme are about 15 times and 9 times higher than those of the fourth-order scheme, respectively.

Besides, the computational memory required by the fourth-order scheme is similar to the classical fourth-order Runge–Kutta (RK) scheme. Further, Appendix A shows that both the fourth-order and the RK schemes have similar numerical behavior. From Appendix A it is found that the amplitude error for the RK scheme is smaller than that for the explicit fourth-order ((4, 4)) scheme. However, the amplitude errors for both schemes are much smaller than their respective phase errors and have little effect on the solution compared with the phase errors, and the phase error for the RK scheme is only slightly smaller than that for the (4, 4) scheme.

Furthermore, compared with the fourth-order RK scheme our explicit fourth-order scheme requires fewer operations per time step and also avoids the difficulty of imposing appropriate intermediate-stage boundary conditions, which are required by the RK scheme to maintain the order of accuracy (see, e.g., [11, 40] and the references quoted there).

2.2. Boundary Conditions

We consider three of the most important boundary conditions: the dielectric interface, the perfect conductor, and a reflectionless absorbing layer to simulate radiation out of a computational domain.

2.2.1. *Reflectionless Absorbing Layers*

To terminate the unbounded domain of scattering problems, we consider the use of a so-called reflectionless absorbing layer technique that was introduced in [41]. In this absorbing layer the absorbing terms are added, in this paper, to the transformed equations other than the original equations so that this takes the form

$$\frac{\partial H^\xi}{\partial t} = -\frac{1}{J\mu}\frac{\partial E^z}{\partial \eta} - \frac{\sigma_\eta^M}{\mu}H^\xi - \frac{\sigma_\xi^M}{\mu^2}R_\eta, \tag{2.21}$$

$$\frac{\partial H^\eta}{\partial t} = \frac{1}{J\mu}\frac{\partial E^z}{\partial \xi} - \frac{\sigma_\xi^M}{\mu}H^\eta + \frac{\sigma_\eta^M}{\mu^2}R_\xi, \tag{2.22}$$

$$\frac{\partial E^z}{\partial t} = \frac{1}{J\epsilon}\left(\alpha\frac{\partial H^\eta}{\partial \xi} - \beta\frac{\partial H^\xi}{\partial \eta}\right) + \frac{1}{J\epsilon}(PH^\xi + QH^\eta) - \frac{\sigma_\xi^E + \sigma_\eta^E}{\epsilon}E^z - \frac{\sigma_\xi^E\sigma_\eta^E}{\epsilon^2}R_z, \tag{2.23}$$

$$\frac{\partial R_\xi}{\partial t} = \frac{1}{J}\frac{\partial E^z}{\partial \xi}, \tag{2.24}$$

$$\frac{\partial R_\eta}{\partial t} = \frac{1}{J}\frac{\partial E^z}{\partial \eta}, \tag{2.25}$$

$$\frac{\partial R_z}{\partial t} = E^z. \tag{2.26}$$

Here $\sigma_\xi^w = 0,\ \sigma_\eta^w = \sigma^w$ in the layers in the η-direction, $\sigma_\eta^w = 0,\ \sigma_\xi^w = \sigma^w$ in the layers in the ξ-direction, and $\sigma_\xi^w = \sigma_\eta^w = \sigma^w$ in the four overlapping corner regions of the absorbing layers, where w denotes M and E. In the case when the reflectionless absorbing layer is needed only in one direction, say, the η direction, choose $\sigma_\xi^w = 0$ and $\sigma_\eta^w = \sigma^w$ with $w = M, E$ and write $R = R_\xi$, so the above equations can be simplified as follows:

$$\frac{\partial H^\xi}{\partial t} = -\frac{1}{J\mu}\frac{\partial E^z}{\partial \eta} - \frac{\sigma^M}{\mu}H^\xi, \tag{2.27}$$

$$\frac{\partial H^\eta}{\partial t} = \frac{1}{J\mu}\frac{\partial E^z}{\partial \xi} + \frac{\sigma^M}{\mu^2}R, \tag{2.28}$$

$$\frac{\partial E^z}{\partial t} = \frac{1}{J\epsilon}\left(\alpha\frac{\partial H^\eta}{\partial \xi} - \beta\frac{\partial H^\xi}{\partial \eta}\right) + \frac{1}{J\epsilon}(PH^\xi + QH^\eta) - \frac{\sigma^E}{\epsilon}E^z, \tag{2.29}$$

$$\frac{\partial R}{\partial t} = \frac{1}{J}\frac{\partial E^z}{\partial \xi}. \tag{2.30}$$

Equations (2.27)–(2.30) are used in the scattering problem by periodic surfaces in Section 3.2 below. The above two sets of equations can be discretized similarly to that shown in Section 2.1.

2.2.2. *Dielectric Interfaces and Perfect Conductors*

We assume the materials involved are nonmagnetic and lossless so that in the TE polarization case the boundary conditions between different dielectric materials become

$$E_1^z = E_2^z, \quad n^x H_1^y - n^y H_1^x = n^x H_2^y - n^y H_2^x, \quad n^x H_1^x + n^y H_1^y = n^x H_2^x + n^y H_2^y, \tag{2.31}$$

where the subscripts refer to the field components in two neighboring media and (n^x, n^y) denotes the unit vector normal to the interface.

Under the orthogonal transformation (2.4) an interface or a boundary in the physical space corresponds to a *ξ-line* where η is constant and ξ varies or an *η-line* where ξ is constant and η varies, so the unit normal to the interface or boundary is $\pm(J/\sqrt{\alpha})\,(\eta_x, \eta_y)$ (when η is constant) or $\pm(J/\sqrt{\beta})\,(\xi_x, \xi_y)$ (when ξ is constant) [32, pp. 74–76]. Without loss of generality we assume that the interface in the physical space corresponds to $\eta = 0$. Then the interface conditions (2.31) become

$$E_1^z = E_2^z, \quad \eta_x H_1^y - \eta_y H_1^x = \eta_x H_2^y - \eta_y H_2^x, \quad \eta_x H_1^x + \eta_y H_1^y = \eta_x H_2^x + \eta_y H_2^y.$$

Due to the orthogonality of the transformation (2.4) these reduce to the simple conditions in the transformed space:

$$E_1^z = E_2^z, \quad H_1^\xi = H_2^\xi, \quad H_1^\eta = H_2^\eta \quad \text{at } \eta = 0. \tag{2.32}$$

If the permittivity ϵ at the interface is evaluated as the average of those at both sides of the interface, that is, $\tilde{\epsilon} = (\epsilon_+ + \epsilon_-)/2$, Yee's second-order scheme can be obtained similarly to that in the interior of the domain. Although this only gives a local truncation error of first-order accuracy, the global second-order convergence rate of the Yee scheme is not affected, as confirmed numerically [58]. However, higher-order approximation formulas at interfaces are needed to match the interior fourth-order scheme. This can be done in the following by employing the technique developed in [53] for the case of a flat interface in the Cartesian coordinate system.

From the interface conditions (2.32) we can conclude the continuity of the time and tangential derivatives of E^z, H^ξ, and H^η (i.e., $\partial E^z/\partial\xi$, $\partial H^\xi/\partial\xi$, and $\partial H^\eta/\partial\xi$) across the interface at $\eta = 0$, so it follows from (2.10) with $\sigma^E = 0$ that

$$\begin{aligned}\frac{\partial E^z}{\partial t} &= \frac{1}{J\epsilon_+}\left(\alpha\frac{\partial H^\eta}{\partial\xi} - \beta\frac{\partial H^\xi_+}{\partial\eta}\right) + \frac{1}{J\epsilon_+}(PH^\xi + QH^\eta)\\ &= \frac{1}{J\epsilon_-}\left(\alpha\frac{\partial H^\eta}{\partial\xi} - \beta\frac{\partial H^\xi_-}{\partial\eta}\right) + \frac{1}{J\epsilon_-}(PH^\xi + QH^\eta)\end{aligned} \tag{2.33}$$

at the interface, where $u\pm$ means the limiting value of $u(t,\xi,\eta)$ as $\eta \to 0\pm$ and similarly for derivatives.

Assume that the electric grid points with $j = 0$ are located at the interface. Since $\partial H^\xi/\partial\eta$ is discontinuous across the interface, then we need to modify its difference approximation at the grids with $j = 0$. To simiplify the expressions, define two vectors $\mathbf{H}_\pm$ by

$$\mathbf{H}_\pm = \big(H^\xi_{i,\pm1/2}, H^\xi_{i,\pm3/2}, H^\xi_{i,\pm5/2}\big).$$

At the grid points $(i,0)$ we use the one-sided third-order difference approximations,

$$\frac{\partial H^\xi_\pm}{\partial\eta} = \pm\frac{1}{\Delta\eta}\big(a_0 H^\xi_{i,0} + \mathbf{a}\cdot\mathbf{H}_\pm\big),$$

where

$$a_0 = -\frac{184}{60}, \quad \mathbf{a} = \frac{1}{60}(225, -50, 9).$$

Substituting these one-sided approximations into (2.33) and eliminating $H^\xi_{i,0}$ we obtain that

$$\begin{aligned}\left.\frac{\partial E^z}{\partial t}\right|_{i,0} &= \frac{b_+ + b_-}{J_{i,0}(b_-\epsilon_- + b_+\epsilon_+)}\\ &\quad\times\left[\alpha_{i,0}\left.\frac{\partial H^\eta}{\partial\xi}\right|_{i,0} - \frac{\beta_{i,0}}{\Delta\eta(b_+ + b_-)}\mathbf{a}\cdot(b_+\mathbf{H}_+ - b_-\mathbf{H}_-) + Q_{i,0}H^\eta_{i,0}\right],\end{aligned}$$

where $b_\pm = a_0\beta_{i,0} \pm \Delta\eta P_{i,0}$. At the grid points immediately next to the interface we may use four-point third-order one-sided approximations:

$$\begin{aligned}\left.\frac{\partial H^\xi}{\partial\eta}\right|_{i,\pm1} &= \pm\frac{1}{24\Delta\eta}\big[-23H^\xi_{i,\pm1/2} + 21H^\xi_{i,\pm3/2} + 3H^\xi_{i,\pm5/2} - H^\xi_{i,\pm7/2}\big],\\ \left.\frac{\partial E^z}{\partial\eta}\right|_{i,\pm1/2} &= \pm\frac{1}{24\Delta\eta}\big[-23E^z_{i,0} + 21E^z_{i,\pm1} + 3E^z_{i,\pm2} - E^z_{i,\pm3}\big].\end{aligned}$$

We can employ the same technique as at interior grid points to discretize the temporal and the other spatial derivatives and to interpolate $H^{\eta}_{i,0}$.

Similarly, at the grid points on and immediately next to a perfectly conducting boundary, which corresponds to $\xi = constant$ or $\eta = constant$ in the transformed space, we may apply four-point third-order one-sided approximations to the spatial derivatives in the ξ or η direction. The temporal and the other spatial derivatives may be discretized by using the same technique as at interior grid points. It should be remarked that similar one-sided difference approximations have also been used in [58], where five-point fourth-order one-sided difference approximations are combined with fifth-order one-sided interpolations to derive fourth-order boundary schemes near boundaries and interfaces.

Numerical experiments in Section 3 showed no instabilities of the fourth-order scheme with the above treatment of interface and boundary conditions. Furthermore, the overall fourth-order convergence rate of the fourth-order scheme was not affected by the above third-order difference schemes at and near the boundaries and interfaces, as confirmed in the numerical experiments in Section 3, which is consistent with the theoretical results of Gustafsson [24, 25].

3. NUMERICAL EXPERIMENTS

To illustrate the performance of the fourth-order scheme we consider in this section two electromagnetic wave problems: the modeling of a cylindrical PEC resonator for which exact solutions exist, and problems of scattering from periodic surfaces.

All the results were computed using MATLAB. The time-step δt in the fourth-order scheme is required to satisfy

$$\delta t \le \frac{4\Delta_{min}}{7\sqrt{2}c},$$

where Δ_{min} is the minimum grid spacing in the x and y directions and $c = \max_{i,j} c_{ij}$, with $c_{ij} = (\mu_{ij}\epsilon_{ij})^{-1/2}$ being the local speed of the wave in the cell (i, j), following the stability analysis in [53] on an infinite homogeneous domain.

3.1. Modeling of Cylindrical PEC Resonators

Assume that the resonator consists of two concentric PEC cylinders with an electromagnetic wave bouncing back and forth between the walls (see Fig. 1). The material is taken to be in a vacuum, (i.e., $\epsilon = \mu = 1$ in normalized units). The radii of the two cylinders are $r_1 = 1/6$ and $r_2 = 1/2$. The exact time-domain solution of the problem is (cf. [1])

$$\begin{aligned}
E^z &= \cos(\omega t + \theta)[J_1(\omega r) + aY_1(\omega r)],\\
H^x &= -\frac{1}{2}\sin(\omega t + \theta)\sin\theta[J_0(\omega r) - J_2(\omega r) + a(Y_0(\omega r) - Y_2(\omega r))]\\
&\quad - \frac{\cos\theta}{\omega r}\cos(\omega t + \theta)[J_1(\omega r) + aY_1(\omega r)],\\
H^y &= \frac{1}{2}\sin(\omega t + \theta)\cos\theta[J_0(\omega r) - J_2(\omega r) + a(Y_0(\omega r) - Y_2(\omega r))]\\
&\quad - \frac{\sin\theta}{\omega r}\cos(\omega t + \theta)[J_1(\omega r) + aY_1(\omega r)]
\end{aligned}$$

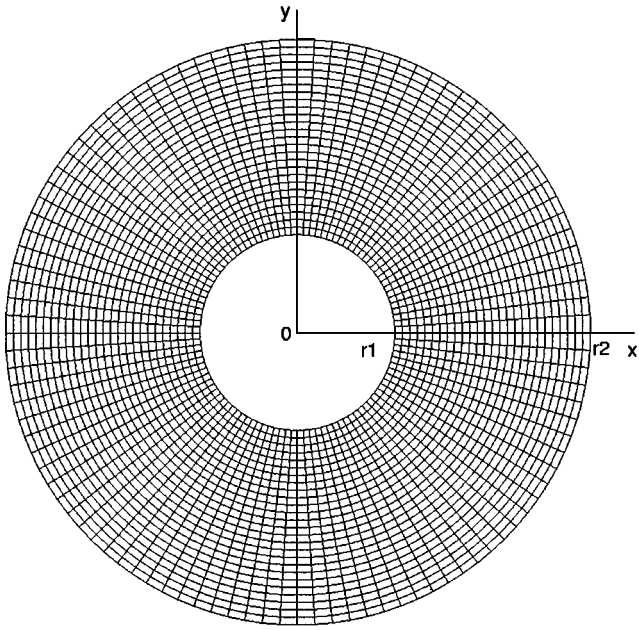

FIG. 1. The cylindrical PEC resonator.

for $r_1 < r < r_2$, where (r, θ) denote the usual polar coordinates, J_n and Y_n stand for the nth order Bessel functions of the first and second kind, respectively, and $\omega = 9.813695999428405$ and $a = 1.76368380110927$, which are obtained from the boundary conditions on the walls at $r = r_1$ and $r = r_2$, respectively, with $E^z = 0$. In this case, the orthogonal curvilinear coordinate (ξ, η) can be taken so that

$$r = r_1 + \frac{\xi - 1}{i_{max} - 1}(r_2 - r_1), \quad \theta = 2\pi \frac{\eta - 1}{j_{max} - 1},$$

where i_{max} and j_{max} denote the number of grid points located equally along the radial (ξ) and angular (η) directions, respectively, with $\Delta\xi = \Delta\eta = 1$. Thus the annulus region in the physical space is mapped onto the rectangular domain $1 < \xi < i_{max}$ and $1 \le \eta \le j_{max}$ in the transformed space.

Figure 2 shows the L_2 error of the electric field component as a function of time, as computed using the Yee and the fourth-order schemes for different resolutions, where h denotes the spatial grid size ($=\pi/156$, $\pi/312$, and $\pi/636$) and the L_2 error is defined by

$$L_2(t) = \sqrt{\frac{\sum_{i=1}^{imax} \sum_{j=1}^{jmax} \left(E^z_{exact}\big|_{i,j} - E^z_{num}\big|_{i,j} \right)^2}{i_{max} j_{max}}}.$$

Table I gives the L_2-error of the electric field component as computed using the Yee and fourth-order schemes on orthogonal curvilinear grids as well as the Yee scheme (with a staircased approximation to the boundary) and the bounded error scheme with simultaneous approximation terms (SAT) developed in [1] for a Cartesian grid. Note that in Table I the results for the staircased Yee scheme and SAT were taken from Ref. [1]. From Table I it is found that the staircase approximation leads to an extremely slow convergence rate at early time ($t = 1$) and a divergent scheme at late time (e.g., $t = 10$). This is probably not only

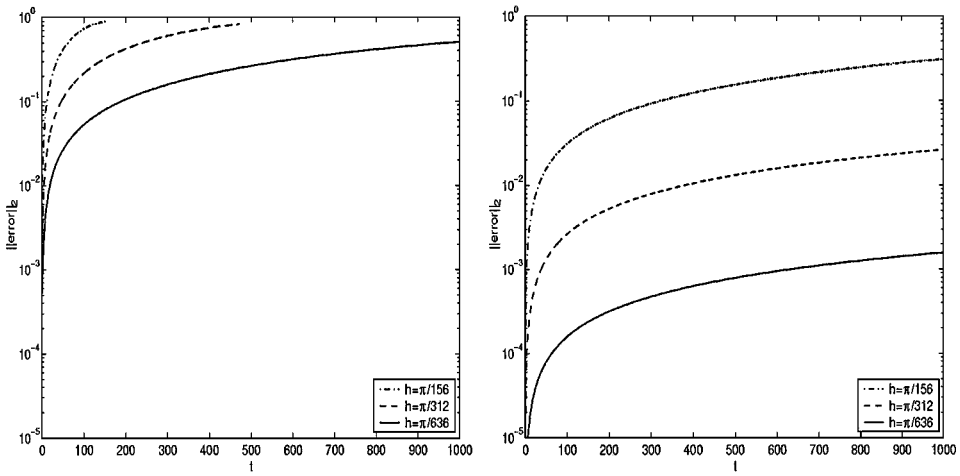

FIG. 2. The L_2 error of E^z vs time t as computed by the curvilinear grid Yee (left) and fourth-order (right) schemes for different resolutions: $h = \pi/156, \pi/312, \pi/636$.

because staircasing misrepresents the shape of the body, but also because of the fact that in this resonator case an electromagnetic wave is bouncing back and forth between the walls, so numerical errors would accumulate quickly in the solution. In contrast, the curvilinear Yee and fourth-order schemes represent the shape of the body exactly and give an excellent convergence rate even at late time, with the (4, 4) scheme performing much better than the Yee scheme (see Fig. 2 and Table I).

3.2. Scattering by Periodic Surfaces

We now consider two-dimensional electromagnetic scattering by a dielectric interface in the transverse electric (TE) polarization case. The model equations are given by (2.1)–(2.3)

TABLE I
The L_2 Error of the Electric Field for Different Schemes under the Cartesian and Curvilinear Coordinates for Different Resolutions

Scheme		h	δt	Grid	$t = 1$ L_2	$t = 1$ Rate	$t = 10$ L_2	$t = 10$ Rate
Cartes.	Yee	$1/40$	$2h/3$	≈1000	0.4322		0.5101	
coord.[a]	(staircase)	$1/80$		≈4000	0.3635	0.28	0.4364	0.23
		$1/160$		≈16000	0.1742	1.06	0.6683	−0.61
	SAT	$1/40$	$h/5$	≈1000	1.203×10^{-3}		8.435×10^{-3}	
		$1/80$		≈4000	1.705×10^{-4}	2.82	8.354×10^{-4}	3.34
		$1/160$		≈16000	1.502×10^{-5}	3.50	8.27×10^{-5}	3.34
Curv.	Yee	$\pi/156$	$h/\sqrt{2}$	676	8.87×10^{-3}		8.65×10^{-2}	
coord.		$\pi/312$		2704	2.24×10^{-3}	1.99	2.20×10^{-2}	1.97
		$\pi/636$		11236	5.51×10^{-4}	2.02	5.35×10^{-3}	2.04
	(4, 4)	$\pi/156$	$2h/5$	676	3.68×10^{-4}		3.14×10^{-3}	
		$\pi/312$		2704	3.30×10^{-5}	3.48	2.67×10^{-4}	3.56
		$\pi/636$		11236	2.22×10^{-6}	3.89	1.63×10^{-5}	4.03

[a] Results in the Cartesian coordinate case were taken from Ref. [1].

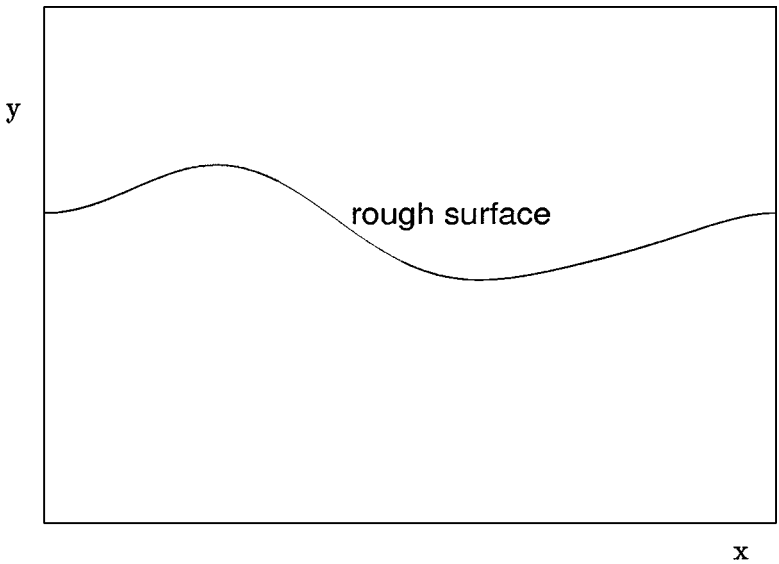

FIG. 3. The computational domain of the scattering problem.

in a Cartesian coordinate system (x, y), and a computational domain is shown in Fig. 3. Periodic boundary conditions are imposed on the two vertical boundaries of the computational domain to allow the study of long-term behavior, whereupon the interface is assumed to be a periodic surface.

The problem of electromagnetic wave scattering from periodic surfaces has been extensively investigated (see, e.g., [7, 14, 15, 17, 27, 30, 42, 51] and the references quoted there). However, almost all of the past work has been in frequency domain using the Floquet theory. To obtain the time-domain response, one has to Fourier transform the frequency domain results, which is not efficient for wideband applications.

The FDTD method provides a good alternative for the solution of scattering problems in the time domain without resorting to frequency-domain analysis. This method has been successfully applied to scattering problems where the scatterer is of finite size (see, e.g., [43, 44] and the references quoted there). Recently the method was also applied to the problem of electromagnetic wave scattering by periodic surface [14, 30, 51], where only the second-order schemes are considered, which suffer from strong numerical dispersion leading to nonphysical oscillations of the solution.

Here we apply the fourth-order orthogonal curvilinear grid FDTD scheme to scattering from periodic surfaces. The numerical results show that the fourth-order scheme is not only numerically stable but also accurate and highly efficient compared with the second-order scheme.

The computational domain is shown in Fig. 3. A perfect conductor is assumed at the top boundary, a reflectionless absorbing layer is used at the bottom boundary, and periodic boundary conditions are used for the side boundaries of the computational domain. Electromagnetic boundary conditions (continuity of tangential electric and magnetic fields) are employed along the rough interface.

The size of the computational domain is assumed to be 10 cm by 10 cm or 0.1 m by 0.1 m ($0 \le x \le 0.1$, $-0.01 \le y \le 0.09$), which is divided equally by a cosine interface with period and peak-height dimensions of 10 and 0.5 cm, respectively. The bottom medium is

assumed to be a free space and the top medium is an isotropic and lossless material of relative permittivity 9 and relative permeability 1, with a perfect conductor at the top ($y = 0.9$) and a reflectionless absorbing layer ($-0.01 < y < 0$) at the bottom. The conductivity of the layer is

$$\sigma(y) = \sigma_m \left(\frac{y}{\delta}\right)^2, \quad \sigma_m = -\frac{3\ln(0.001)}{2\delta}\epsilon_0 c,$$

where $\delta = 0.01$ m is the thickness of the layer, ϵ_0 is the permittivity of the free space, and c is the speed of light. The normal incident pulse (along y direction) is taken to be a Gaussian of the form [51]

$$E_z(t, y) = \exp\left[-\left(\frac{t - y/c}{pw}\right)^2\right], \tag{3.34}$$

where $pw = 26$ ps.

The problem was solved by three methods: the Yee scheme with a staircased approximation to the interface, and the Yee ((2, 2)) and fourth-order ((4, 4)) schemes on an orthogonal curvilinear grid conforming to the interface. The conformal orthogonal curvilinear grid is generated using the numerical grid generation technique proposed in Appendix B along with the blending function (B.6) (see Fig. 4b). Since the exact solution for this problem is unknown, the numerical solution obtained using the staircased Yee scheme on a fine uniform Cartesian grid with the grid size $\Delta x = \Delta y = 0.0083$ cm (1200 grid points in both directions) is assumed to be the exact solution. This reference solution is compared with the numerical solution computed using the curvilinear Yee and fourth-order schemes for different resolutions. The Courant number ν is taken to be 0.4 for all three schemes, so the time step is taken as $\delta t = \nu \Delta x/c = 0.11113$ ps for the staircased Yee scheme, $\delta t = \nu \min(\Delta x)/c = 0.78277$, 0.39139, and 0.195695 ps for the curvilinear Yee scheme with resolutions 100×100, 200×200, and 400×400, respectively, and $\delta t = \nu \min(\Delta x)/c = 0.78277$ and 0.39139 ps for the curvilinear fourth-order scheme with resolutions 100×100 and 200×200, respectively.

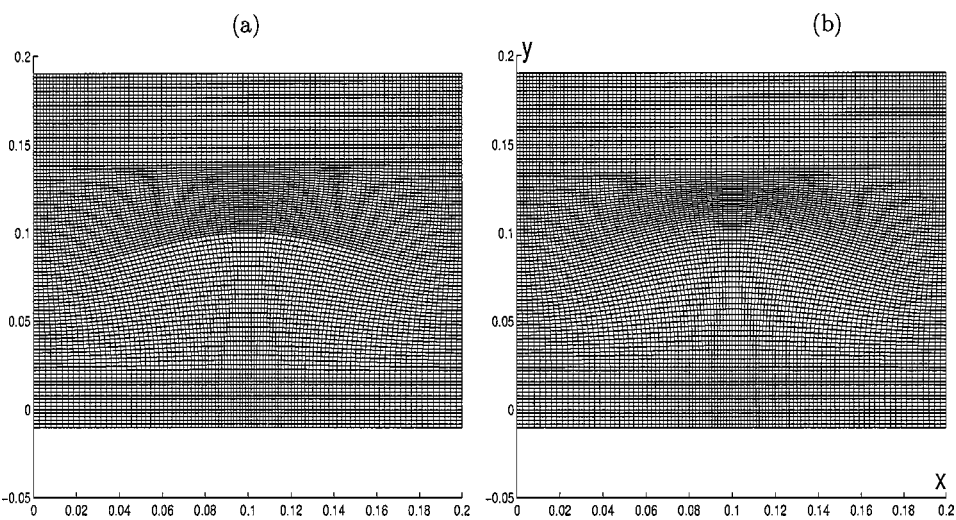

FIG. 4. Orthogonal curvilinear grids conforming to the interface and generated using the blending functions ω given by (B.5) (a) and (B.6) (b).

TABLE II

Comparison of CPU Time, Memory, L_2 Error, and Convergence Rate for the Staircased Yee Scheme and the Curvilinear Yee and Fourth-Order Schemes with Different Resolutions

Scheme	Grid	CPU time (min)	Memory (meg)	$t = 1000$ ps $\|Error\|_2$	Rate
(2, 2)	100×100	1.38	7.16	5.59×10^{-2}	
	200×200	11.4	28.4	1.85×10^{-2}	1.59
	400×400	95.1	113	3.96×10^{-3}	2.23
(4, 4)	100×100	6.28	12.4	7.88×10^{-3}	
	200×200	54.5	49.1	5.59×10^{-4}	3.82
Staircased	100×100	0.57	3.12	6.54×10^{-2}	
Yee	200×200	4.61	12.3	2.37×10^{-2}	1.46
	400×400	41.9	49.0	5.77×10^{-3}	2.04
	800×800	317	195	9.10×10^{-4}	
	1200×1200	1063	441		

Table II compares the CPU time and memory as well as the L_2 error and the convergence rate for the staircased Yee and the curvilinear Yee and fourth-order schemes for different resolutions at $t = 1000$ ps. Table II shows the fourth-order and second-order convergence rates of the curvilinear fourth-order and Yee schemes. It is further found from Table II that to achieve the same level of numerical error the CPU time and memory requirements of the curvilinear fourth-order scheme are about 15 and 9 times lower than those of the curvilinear Yee scheme, respectively, and about 7 and 4 times lower than those of the staircased Yee scheme, respectively.

For testing the stability of the curvilinear Yee and fourth-order schemes in conjunction with the reflectionless absorbing layer and the numerical treatment of the boundary and interface conditions, the computation was further carried out up to $t = 10{,}000$ ps (over 12,775 time steps).

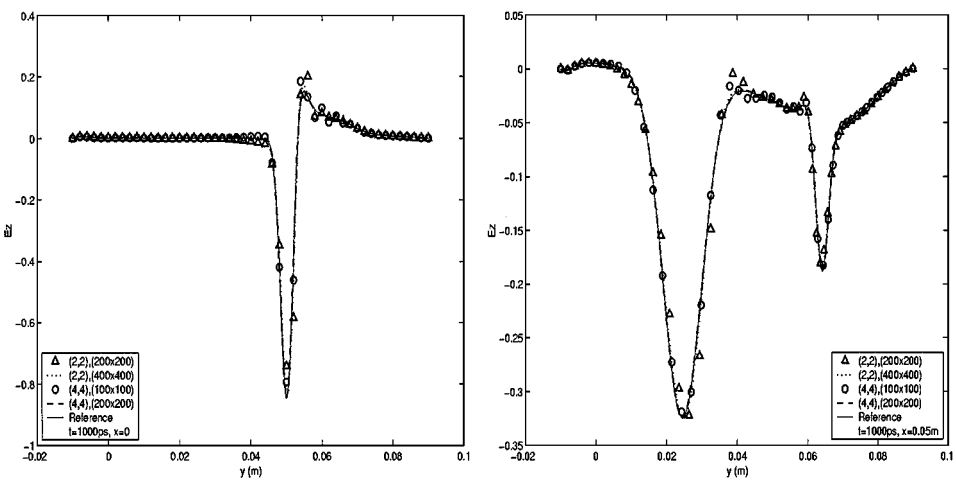

FIG. 5. Gaussian pulse normally hitting a sinusoidal interface. Distribution of the electric field at $t = 1000$ ps along $x = 0$ (left) and $x = 0.05$ m (right) as computed by the curvilinear Yee and (4, 4) schemes for different resolutions.

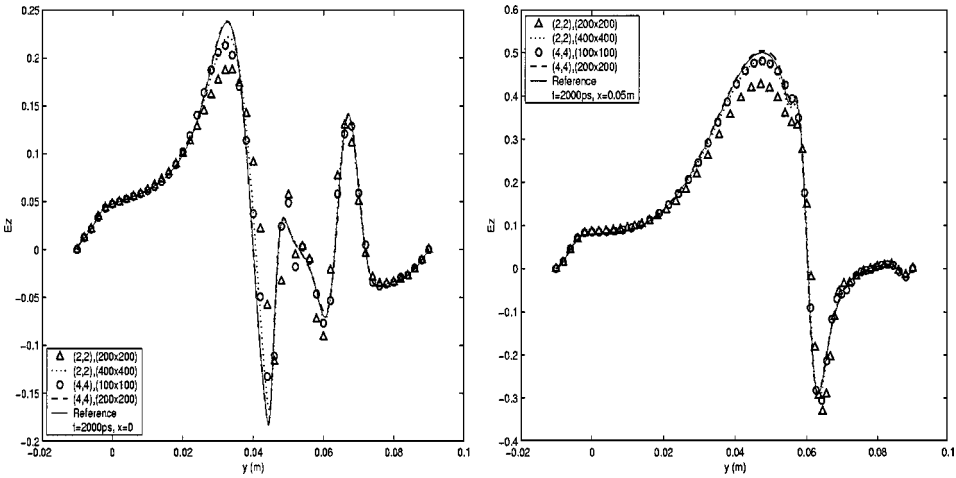

FIG. 6. Gaussian pulse normally hitting a sinusoidal interface. Distribution of the electric field at $t = 2000$ ps along $x = 0$ (left) and $x = 0.05$ m (right) as computed by the curvilinear Yee and (4, 4) schemes for different resolutions.

The electric field distribution is recorded at $t = 1000$, 2000, and 10,000 ps and shown in Figs. 5, 6, and 7. The numerical results computed using the fourth-order scheme with the resolution 200×200 are found to be in excellent agreement with the reference solution even at a very late time (e.g., $t = 10{,}000$ ps). However, the numerical results computed using the fourth-order scheme with the low-resolution 100×100 and the Yee scheme with the high-resolution 400×400 are found to be in good agreement with each other at all times up to $t = 10{,}000$ ps but have some discrepancies with the reference solution even at early time (e.g., $t = 2000$ ps). No instability was observed in the numerical computations.

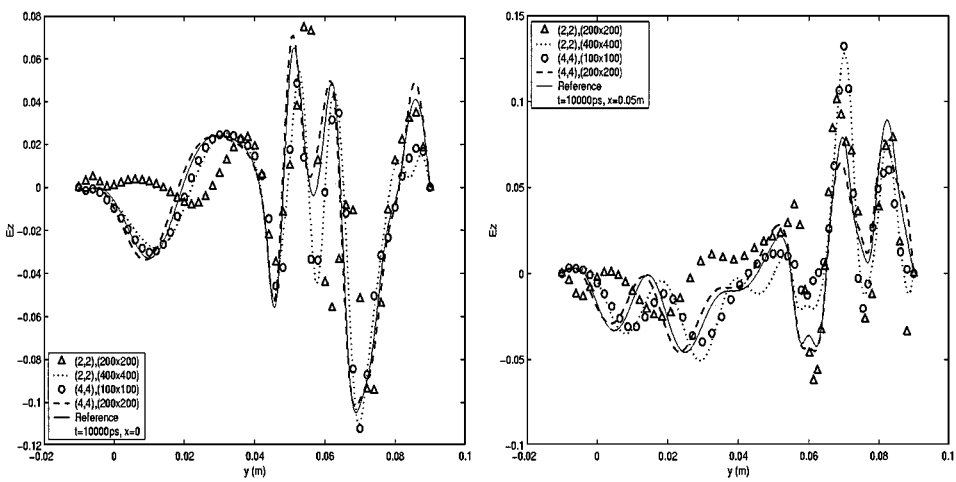

FIG. 7. Gaussian pulse normally hitting a sinusoidal interface. Distribution of the electric field at $t = 10{,}000$ ps along $x = 0$ (left) and $x = 0.05$ m (right) as computed by the curvilinear Yee and (4, 4) schemes for different resolutions.

4. CONCLUSIONS

The explicit fourth-order accurate staggered FDTD scheme, proposed in [53] for Maxwell's equations in a Cartesian grid, has been extended to an orthogonal curvilinear grid which conforms to metallic boundaries and dielectric interfaces so it can be applied to complex electromagnetic structures. The fourth-order scheme has been extended to the reflectionless absorbing layer simulating radiation out of a computational domain. The associated third-order boundary schemes have also been described for two classes of boundary conditions: the dielectric interface and the perfect conductor. The advantage of using orthogonal curvilinear grids is that the simple structure of Maxwell's equations is remained in the transformed equations and the boundary and interface conditions are greatly simplified.

The method has been applied to scattering from periodic surfaces, and a simple technique has also been presented for generating orthogonal curvilinear grids that conform to the material boundaries and interfaces in the scattering problem. Numerical results indicate that the fourth-order scheme is numerically stable and is efficient in modeling electromagnetic scattering from periodic surfaces.

The method has also been applied to a problem of modeling a cylindrical PEC resonator consisting of two concentric PEC cylinders with an electromagnetic wave bouncing back and forth between the walls. From the results it is clear that the staircase approximation may not be appropriate in computation of microwave resonators due to the extremely slow convergence even at a early time of staircased schemes and the new fourth-order scheme on an orthogonal curvilinear grid can be an effective alternative.

For problems involving nonsmooth or random rough surfaces it is difficult to generate orthogonal curvilinear grids. Currently work is in progress in extending the algorithm to deal with these cases. On the other hand, although numerous computational experiments have shown no instabilities whatsoever, this remains an interesting open question.

APPENDIX A: STABILITY, DISPERSION, AND DISSIPATION

In this appendix we discuss the stability, dispersion, and dissipation of the interior fourth-order scheme for the one-dimensional case with an infinite homogeneous lossless computational domain in the Cartesian coordinate system (see [53] for details). In this case, our fourth-order scheme leads to the characteristic equation for λ of

$$576\lambda^5(\lambda-1)^2+(PQ)^2(26\lambda^3-5\lambda^2+4\lambda-1)^2=0, \tag{A.1}$$

where $P=\nu\sin(k\Delta x/2)$ and $Q=(6+\sin^2(k\Delta x/2))/3$, with the Courant (or CFL) number $\nu=c\delta t/\Delta x$ and $c=(\epsilon\mu)^{-1/2}$, λ is the complex time eigenvalue whose magnitude will determine the stability and dissipation properties of the difference scheme, and k is the real wavenumber of the arbitrary harmonic wave component whose stability and decay is determined by $|\lambda|$. The solutions of (A.1) give λ as a function of the medium parameters, the time step, and the quantity $k\Delta x=2\pi/N$ (with N being the number of points per wavelength).

It was shown in [53] that $\max|\lambda|\le 1$ for arbitrary Δx as long as $\nu\le 4/7$ and, hence, the fourth-order difference scheme is stable in the one-dimensional homogeneous case as long as $\nu=c\delta t/\Delta x\le 4/7\approx 0.57$. Note that in the two-dimensional homogeneous case

the stability condition for the fourth-order scheme is [53]:

$$\sqrt{\left(\frac{c\delta t}{\Delta x}\right)^2 + \left(\frac{c\delta t}{\Delta y}\right)^2} \le \frac{4}{7}. \tag{A.2}$$

The solution λ of the characteristic equation (A.1) in the 1-D case determines the dispersion and dissipation properties of the fourth-order scheme; $|\lambda|$ determines the amplitude (or dissipative) error, while $\arctan(\Im\lambda/\Re\lambda)$ determines the phase (or dispersive) error, where $\Im\lambda$ and $\Re\lambda$ are the imaginary and real parts of λ. The normalized local amplitude and phase errors are determined from the principal root λ that is an approximation to $\exp(i\omega\delta t) = \exp(ick\delta t)$ using

$$er_a = |\lambda| - 1, \tag{A.3}$$

$$er_p = 1 + \frac{\phi}{\omega\delta t} = 1 + \frac{\phi}{\nu k\Delta x}, \tag{A.4}$$

where $\phi = \arctan(\Im\lambda/\Re\lambda)$. Figure 8 plots the normalized local amplitude (or dissipative) errors for the (4, 4) and RK schemes as a function of spatial resolution $k\Delta x$ at a Courant number of 0.4, where the RK scheme employs the classical fourth-order four-stage Runge–Kutta time integrator in conjunction with the five-point fourth-order central difference approximations to the first-order spatial derivatives (see, e.g., [60]); note that the Yee scheme is dissipationless. From Fig. 8 it is seen that the amplitude error for the RK scheme is smaller than that for the (4, 4) scheme. For example, when the wave is sampled at eight points per wavelength the amplitude errors for the RK and the (4, 4) schemes are -0.00065% and

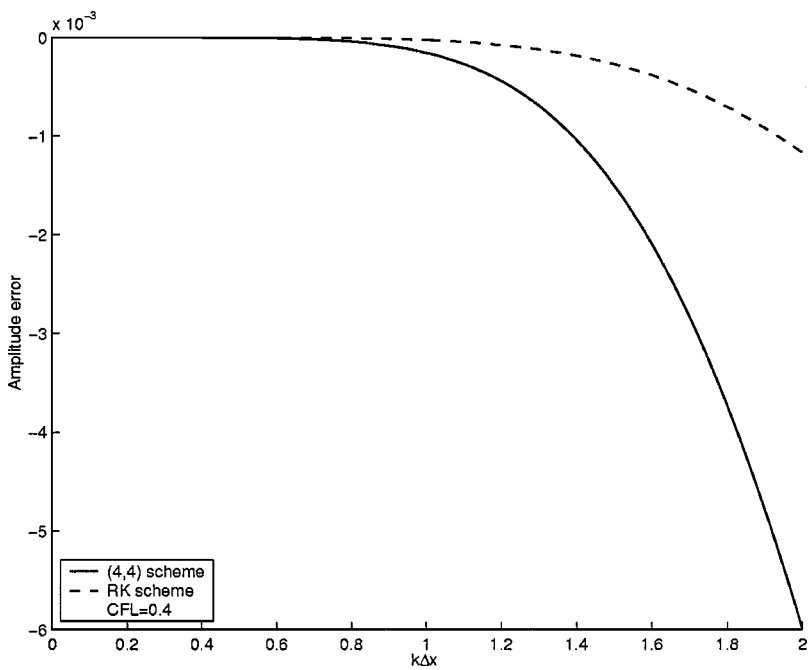

FIG. 8. Amplitude (or dissipative) errors for the (4, 4) and the RK schemes as a function of spatial resolution $k\Delta x$ at a Courant number of 0.4.

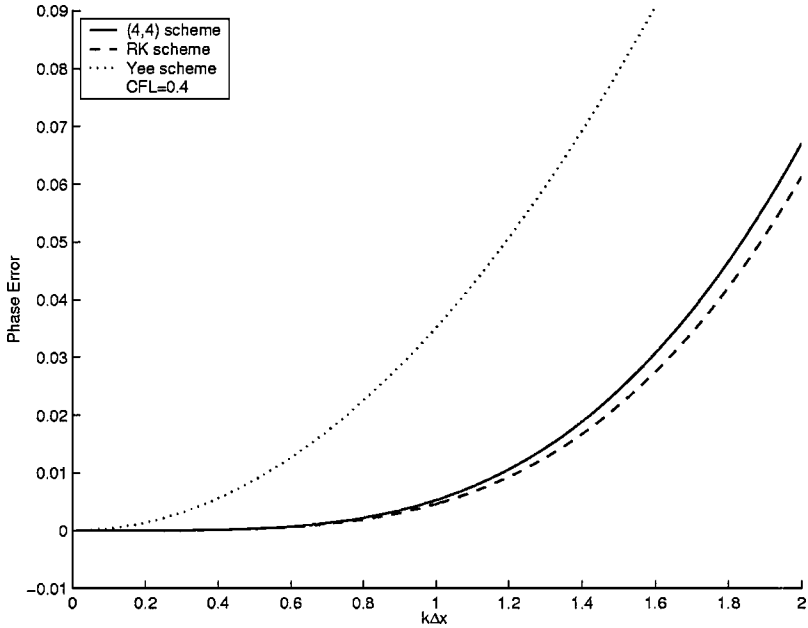

FIG. 9. Phase (or dispersive) errors for the Yee, (4, 4) and RK schemes as a function of spatial resolution $k\Delta x$ at a Courant number of 0.4.

-0.00384%, respectively. However, the amplitude errors for both schemes are much smaller than their respective phase errors, as seen from Fig. 9, where the phase errors are ploted as a function of the spatial resolution at a Courant number of 0.4 for the Yee, (4, 4) and RK schemes, and the phase error for the RK scheme is only slightly smaller than that for the (4, 4) scheme. For example, if the wave is sampled at eight points per wavelength (i.e., $k\Delta x = \pi/4$), the phase errors for the Yee, (4, 4), and RK schemes are 0.0217, 0.00207, and 0.00179 rad, respectively. Conversely, for Yee's scheme to achieve a phase error of 0.002 rad the wave needs to be sampled at 26.3 points per wavelength (i.e., $k\Delta x = 0.239$).

APPENDIX B: ORTHOGONAL GRID GENERATION

Numerical grid generation is a rapidly developing area in scientific computation [32, 49] and has become an essential part of computational fluid dynamics, electromagnetics, and the like. Its use gives to finite-difference and finite-volume methods capabilities for modeling realistic geometries similar to those of the finite-element method and extends computational modeling of fluid flow and electromagnetic waves and fields to engineering analysis and design. In this appendix, we propose a simple technique to generate orthogonal curvilinear grid for domains containing curved interfaces or boundaries based on the idea that if the slope of a given curve passing through a point (x_0, y_0) is $g(x_0, y_0)$, then the perpendicular trajectory through this point has slope $-1/g(x_0, y_0)$ [33].

Orthogonal grid generation has been studied by many authors in two- and three-dimensional cases, including doubly connected regions (see, e.g., [3, 5, 19, 32, 47–49, 52] and the references quoted there). Our method is much simpler compared with the previous ones and can be applied to problems involving duct-shaped domains, such as scattering by rough surfaces, including periodic surfaces (diffraction gratings), wave propagation

and scattering in multilayered media with curved boundaries and interfaces, duct acoustic problems, and so on. Note that orthogonal grids have been used recently for numerically solving a problem in the duct acoustics in [4] as well as electromagnetic wave problems in multilayered regions with curved boundaries and interfaces in [34, 39].

Consider the computational domain shown in Fig. 3. Suppose the interface is given by the function $y = y_{in}(x)$ and the top bottom boundaries are parallel to the x-axis and defined by $y = y_{top} = constant$ and $y = y_{bottom} = constant$, respectively. These three grid lines correspond to three ξ-lines (i.e., $\eta = constant$) and may be determined first. Let $g(x, y)$ denote the slop of the grid lines at which $\eta = const$, that is,

$$g(x, y) = \left.\frac{dy}{dx}\right|_{\eta=const}. \tag{B.1}$$

Then the slope of the perpendicular trajectory through (x, y) is $-1/g(x, y)$ so that

$$g(x, y) = -\left.\frac{dx}{dy}\right|_{\xi=const}. \tag{B.2}$$

The above two equations may be solved for grid lines, and there are an infinite number of choices for g. However, certain conditions must be imposed on g so as to get a conformal grid to the interface and boundaries. Define the interface and the top and bottom boundaries by

$$\Gamma_{in} := \{(x, y)|y = y_{in}(x)\},$$
$$\Gamma_s := \{(x, y)|y = y_s\},$$

where s stands for *top* or *bottom*. Then it follows that

$$g(x, y) = y'_{in}(x), \quad (x, y) \in \Gamma_{in}, \tag{B.3}$$
$$g(x, y) = 0, \quad (x, y) \in \Gamma_s. \tag{B.4}$$

For simplicity, define

$$g(x, y) = \omega(\Delta, \delta)\Delta'$$

where the blending function ω satisfies that $\omega(\Delta, 0) = 0$ and $\omega(\Delta, \Delta) = 1$, and

$$\delta(y) = y - y_s, \quad \Delta(x) = y_{in}(x) - y_s, \quad \Delta' = \frac{d\Delta}{dx} = y'_{in}(x),$$

with y_s representing y_{top} or y_{bottom}. Clearly, g satisfies the conditions (B.3) and (B.4). The simplest choice for g is

$$\omega(\Delta, \delta) = \frac{\delta}{\Delta}. \tag{B.5}$$

Figure 4a shows a sample mesh generated using this choice for ω. The grid conforms to the interface and boundaries. However, the size of the grid varies sharply at the interface and the joint line between curvilinear and linear coordinates, which results in jumping of grid

derivatives and then extra computational error. This is because the choice (B.5) for ω as a function of δ has discontinuous derivatives at 0 and Δ. A better choice for ω may be

$$\omega(\Delta, \delta) = \frac{1}{2}\left[1 - \cos\left(\frac{\delta}{\Delta}\pi\right)\right], \tag{B.6}$$

which is smooth at $\delta = 0, \Delta$. Figure 4b shows the grid mesh generated with this function, which is stretched nicely in the whole domain compared with that shown in Fig. 4a and will lead to better numerical results.

The procedure of the numerical grid generation is as follows:

1. Determine the blending function ω in the whole domain.
2. Locate the grid points (x_i, y_i) at the interface, $x_i = i\Delta x$, $y_i = y_{in}(x_i)$, where $i = 1, 2, \ldots, i_{max}$, and then solve the ordinary differential equation (B.2) with the starting value (x_i, y_i) and the finishing value y_s to get a group of mesh lines.
3. Locate the grid points (x_j, y_j) at the left boundary, $x_j = 0, y_j = y_{in}(0) + (j - j_{in})\Delta y$, where $j = 1, 2, \ldots, j_{max}$ and $\eta = j_{in}$, corresponding to the interface, and then solve the ordinary differential equation (B.1) with the starting value (x_j, y_j) and the finishing value x_r to get another group of mesh lines, where x_r is the value of x at the right boundary.
4. Solve for the grid points from the intersections of two sets of mesh lines.

Numerical methods may be used to solve the differential equations in steps 2 and 3. In generating the grids shown in Fig. 4 the Runge–Kutta method was used in this paper to solve the differential equations in steps 2 and 3.

APPENDIX C: CALCULATION OF GRID DERIVATIVES

Grid derivatives appear in the transformed Maxwell's equations so it is important to calculate accurately the values of these grid derivatives in order to match the accuracy of the fourth-order scheme. The function $g(x, y)$ is given everywhere in the domain and can be used effectively to determine the grid derivatives. To this end, we derive certain relations between g and the grid derivatives. First it follows from (B.1) and (B.2) that

$$x_\eta = \frac{\partial x}{\partial \eta} = \left.\frac{dx}{dy}\right|_{\xi=const} \frac{\partial y}{\partial \eta} = -g(x, y)y_\eta, \tag{C.1}$$

$$y_\xi = \frac{\partial y}{\partial \xi} = \left.\frac{dy}{dx}\right|_{\eta=const} \frac{\partial x}{\partial \xi} = g(x, y)x_\xi. \tag{C.2}$$

Next, by a direct calculation it can be obtained that

$$P = 2(g_1 + gg_2)x_\xi^2 y_\eta, \tag{C.3}$$

$$Q = 2(g_2 - gg_1)x_\xi y_\eta^2, \tag{C.4}$$

where $g_1 = \frac{\partial g(x,y)}{\partial x}$ and $g_2 = \frac{\partial g(x,y)}{\partial y}$.

From (C.1)–(C.4) it is seen that the calculation of the grid derivatives that appeared in our fourth-order scheme (i.e., in α, β, J, P, and Q) reduces to that of the two simplest first-order grid derivatives x_ξ and y_η, which may be approximated using the five-point fourth-order centered difference schemes (2.19)–(2.20) (see Section 2.1).

ACKNOWLEDGMENTS

The authors thank the referees and the associate editor for their invaluable comments and suggestions which helped improve the paper greatly.

REFERENCES

1. S. Abarbanel, A. Ditkowski, and A. Yefet, *Bounded Error Schemes for the Wave Equation on Complex Domains*, ICASE Report No. 98-50 (NASA Langley Research Center, Hampton, 1998).
2. S. Abarbanel and D. Gottlieb, On the construction and analysis of absorbing layers in CEM, *Appl. Numer. Math.* **27**, 331 (1998).
3. L. Abrahamsson, Orthogonal grid generation for the two-dimensional ducts, *J. Comput. Appl. Math.* **34**, 305 (1991).
4. L. Abrahamsson and H.-O. Kreiss, Numerical solution of the coupled mode equations in duct acoustics, *J. Comput. Phys.* **111**, 1 (1994).
5. A. Allievi and S. M. Calisal, Application of Bubnov-Galerkin formulation to orthogonal grid generation, *J. Comput. Phys.* **98**, 163 (1992).
6. J. J. Ambrosiano, S. T. Brandon, R. Löhner, and C. R. DeVore, Electromagnetic via the Taylor–Galerkin finite element method on unstructured grids, *J. Comput. Phys.* **110**, 310 (1994).
7. M. Bagieu and D. Maystre, Waterman and Rayleigh methods for diffraction grating problems: Extension of the convergence domain, *J. Opt. Soc. Am.* **A15**, 1566 (1998).
8. A. Bayliss, K. E. Jordan, B. J. LeMesurier, and E. Turkel, A fourth-order accurate finite difference scheme for the computation of elastic waves, *Bull. Seismol. Soc. Am.* **76**, 1115 (1986).
9. J. P. Berenger, A perfectly matched layer for the absorption of electromagnetic waves, *J. Comput. Phys.* **114**, 185 (1994).
10. A. C. Cangellaris and D. B. Wright, Analysis of the numerical error caused by the stairstepped approximation of a conducting boundary in FDTD simulations of electromagnetic phenomena, *IEEE Trans. Antennas Propag.* **39**, 1518 (1991).
11. M. H. Carpenter, D. Gottlieb, S. Abarbanel, and W. S. Don, The theoretical accuracy of Runge–Kutta time discretizations for the initial boundary value problem: A careful study of the boundary error, *SIAM J. Sci. Comput.* **16**, 1241 (1995).
12. M. H. Carpenter, D. Gottlieb, and S. Abarbanel, Stable and accurate boundary treatments for compact, high-order finite-difference schemes, *Appl. Numer. Math.* **12**, 55 (1993).
13. M. H. Carpenter, D. Gottlieb, and S. Abarbanel, Time-stable boundary conditions for finite-difference schemes solving hyperbolic systems: Methodology and application to high-order compact schemes, *J. Comput. Phys.* **111**, 220 (1994).
14. C. H. Chan, S. H. Lou, L. Tsang, and J. A. Kong, Electromagnetic scattering of waves by random rough surface: A finite-difference time-domain approach, *Microwave Opt. Technol. Lett.* **4**, 355 (1991).
15. S. L. Chuang and J. A. Kong, Wave scattering from a periodic dielectric surface for a general angle of incidence, *Radio Sci.* **17**, 545 (1982).
16. G. Cohen and P. Joly, Construction and analysis of fourth-order finite difference schemes for the acoustic wave equation in nonhomogeneous media, *SIAM J. Numer. Anal.* **33**, 1266 (1996).
17. J. DeSanto, G. Erdmann, W. Hereman, and M. Misra, Theoretical and computational aspects of scattering from rough surfaces: One-dimensional perfectly reflecting surfaces, *Waves Random Media* **8**, 385 (1998).
18. T. A. Driscoll and B. Fornberg, Block pseudospectral methods for Maxwell's equations II: Two-dimensional, discontinuous-coefficient case, *SIAM J. Sci. Comput.* **21**, 1146 (1999).
19. R. Duraiswami and A. Prosperetti, Orthogonal mapping in two dimensions, *J. Comput. Phys.* **98**, 254 (1992).
20. J. Fang, *Time Domain Finite Difference Computation for Maxwell's Equations*, Ph.D. Thesis (Univ. California, Berkeley, 1989).
21. J. Fang and J. Ren, A locally conformed finite-difference time-domain algorithm of modeling arbitrary shape palnar metal strips, *IEEE Trans. Microwave Theory Technol.* **41**, 830 (1993).

22. M. Fusco, FDTD algorithm in curvilinear coordinates, *IEEE Trans. Antennas Propag.* **AP-38**, 76 (1990).
23. D. Gottlieb and E. Turkel, Dissipative two-four methods for time-dependent problems, *Math. Comput.* **30**, 703 (1976).
24. B. Gustafsson, The convergence rate for difference approximations to mixed initial boundary value problems, *Math. Comput.* **29**, 396 (1975).
25. B. Gustafsson, The convergence rate for difference approximations to general mixed initial boundary value problems, *SIAM J. Numer. Anal.* **18**, 179 (1981).
26. Y. Hao and C. J. Railton, Analyzing electromagnetic structures with curved boundaries on Cartesian FDTD meshes, *IEEE Trans. Antennas Propag.* **AP-46**, 82 (1998).
27. F. D. Hastings, J. B. Schneider, and S. L. Broschat, A Monte-Carlo FDTD technique for rough surface scattering, *IEEE Trans. Antennas Propag.* **AP-43**, 1183 (1995).
28. R. Holland, Finite difference solutions of Maxwell's equations in generalized nonorthogonal coordinates, *IEEE Trans. Nucl. Sci.* **30**, 4589 (1983).
29. R. Holland, Pitfalls of staircase meshing, *IEEE Trans. Electromagn. Compat.* **35**, 434 (1993).
30. H. Ichikawa, Electromagnetic analysis of diffraction grtings by the finite-difference time-domain method, *J. Opt. Soc. Am. A* **15**, 152 (1998).
31. T. G. Jurgens, A. Taflove, K. Umashankar, and T. G. Moore, Finite-difference time-domain modeling of curved surfaces, *IEEE Trans. Antennas Propag.* **AP-40**, 357 (1992).
32. P. Knupp and S. Steinberg, *Fundamentals of Grid Generation* (CRC Press, Boca Raton, FL, 1993).
33. E. Kreyszig, *Advanced Engineering Mathematics* (Wiley, 1999), 8th ed.
34. E. Larsson, A domain decomposition method for the Helmholtz equation in a multilayer domain, *SIAM J. Sci. Comput.* **20**, 1713 (1999).
35. J. F. Lee, R. Palandech, and R. Mittra, Modeling three-dimensional discontinuities in waveguides using nonorthogonal FDTD algorithm, *IEEE Trans. Microwave Theory Technol.* **MTT-40**, 346 (1992).
36. R. J. LeVeque and C. Zhang, The immersed interface method for acoustic wave equations with discontinuous coefficients, *Wave Motion* **25**, 237 (1997).
37. N. K. Madsen, Divergence preserving discrete surface integral methods for Maxwell's curl equations using nonorthogonal unstructured grids, *J. Comput. Phys.* **119**, 34 (1995).
38. N. K. Madsen and R. W. Ziolkowski, Numerical solution of Maxwell's equations in the time domain using irregular non-orthogonal grids, *Wave Motion* **10**, 583 (1988).
39. K. Otto and E. Larsson, Iterative solution of the Helmholtz equation by a second-order method, *SIAM J. Matrix Anal. Appl.* **21**, 209 (1999).
40. D. Pathria, The correct formulation of intermediate boundary conditions for Runge–Kutta time integration of initial boundary value problems, *SIAM J. Sci. Comput.* **18**, 1255 (1997).
41. P. G. Petropoulos, L. Zhao, and A. C. Cangellaris, A reflectionless sponge layer absorbing boundary condition for the solution of Maxwell's equations with high-order staggered finite difference schemes, *J. Comput. Phys.* **139**, 184 (1998).
42. J. P. Plumey and G. Granet, Generalization of the coordinate transformation method with application to surface-relief gratings, *J. Opt. Soc. Am.* **A16**, 508 (1999).
43. A. Taflove, *Computational Electrodynamics: The Finite-Difference Time-Domain Method* (Artech House, Norwood, MA, 2000), 2nd ed.
44. A. Taflove, *Advances in Computational Electrodynamics: The Finite-Difference Time-Domain Method* (Artech House, Norwood, MA, 1998).
45. A. Taflove and M. E. Brodwin, Numerical solution of steady-state electromagnetic scattering problems using the time-dependent Maxwell's equations, *IEEE Trans. Microwave Theory Technol.* **23**, 623 (1975).
46. A. Taflove, Application of the finite-difference time-domain method to sinusoidal steady-state electromagnetic penetration problems, *IEEE Trans. Electromagn. Compat.* **22**, 191 (1980).
47. P. Tamamidis and D. N. Assanis, Generation of orthogonal grids with control of spacing, *J. Comput. Phys.* **94**, 437 (1991).

48. T. Theodoropoulos and G. C. Bergeles, A Laplace equation method for numerical generation of boundary-fitted 3D orthogonal grids, *J. Comput. Phys.* **82**, 269 (1989).
49. J. F. Thompson, Z. U. A. Warsi, and C. W. Mastin, *Numerical Grid Generation* (Elsevier, Amsterdam/ New York, 1985).
50. E. Turkel and A. Yefet, On the construction of a high order difference scheme for complex domains in a Cartesian grid, *Appl. Numer. Math.* **33**, 113 (2000).
51. M. E. Veysoglu, R. T. Shin, and J. A. Kong, A finite-difference time-domain analysis of wave scattering from periodic surface: oblique incidence case, *J. Electromagn. Waves Appl.* **7**, 1595 (1993).
52. Z. U. A. Warsi and J. F. Thompson, A noniterative method for the generation of orthogonal coordinates in doubly-connected regions, *Math. Comput.* **38**, 501 (1982).
53. Z. Xie, C. H. Chan, and B. Zhang, An explicit fourth-order staggered finite-difference time-domain method for Maxwell's equations, *J. Comput. Appl. Math.*, to appear.
54. B. Yang and D. Gottlieb, Comparisons of staggered and non-staggered schemes for Maxwell's equations, in *Proceedings of the 12th Annual Review of Progress in Applied Comput. Electromagnetics, Naval Postgraduate School, Monterey, CA, 1996*, Vol. II, pp. 1122–1131.
55. K. S. Yee, Numerical solution of initial boundary value problems involving Maxwell's equations in isotropic media, *IEEE Trans. Antennas Propag.* **AP-14**, 302 (1966).
56. K. S. Yee, J. S. Chen, and A. H. Chang, Conformal finite-difference time-domain (FDTD) with overlapping grids, *IEEE Trans. Antennas Propag.* **40**, 1068 (1992).
57. K. S. Yee and J. S. Chen, The finite-difference time-domain (FDTD) and the finite-volume time-domain (FVTD) methods in solving Maxwell's equations, *IEEE Trans. Antennas Propag.* **45**, 354 (1997).
58. A. Yefet and P. G. Petropoulos, A non-dissipative staggered fourth-order accurate explicit finite difference scheme for the time-domain Maxwell's equations, *J. Comput. Phys.* **168**, 286 (2001).
59. A. Yefet and E. Turkel, Fourth-order compact implicit method for the Maxwell equations with discontinuous coefficients, *Appl. Numer. Math.* **33**, 125 (2000).
60. J. L. Young, D. Gaitonde, and J. J. S. Shang, Toward the construction of a fourth-order difference scheme for transient EM wave simulation: Staggered grid approach, *IEEE Trans. Antennas Propag.* **AP-45**, 1573 (1997).